Investigation and characterization of the additive manufacturing of polycaprolactone/bioactive glass hybrid scaffolds for bone tissue engineering via material extrusion processing

Lukas Gritsch, Haroutioun Askanian, Vera Bednarzig, Stefan Schrüfer, Joachim Kaschta, Christelle Blavignac, Steve Peuble, Frédéric Gallice, Edouard Jallot, Aldo R. Boccaccini, et al.

Investigation and characterization of the additive manufacturing of polycaprolactone/bioactive glass hybrid scaffolds for bone tissue engineering via material extrusion processing".

Lukas Gritsch[1,2,4,*], Haroutioun Askanian[3], Vera Bednarzig[4], Stefan Schrüfer[5], Joachim Kaschta[5], Christelle Blavignac[6], Steve Peuble[7,8], Frédéric Gallice[7,8], Edouard Jallot[1], Aldo R. Boccaccini[4] and Jonathan Lao[1]

Affiliations

[1] Laboratoire de Physique de Clermont (LPC), UMR 6533, Université Clermont Auvergne, 63000, Clermont-Ferrand, France

[2] Technogym S.P.A., 47521, Cesena, Italy

[3] Institut de Chimie de Clermont Ferrand (ICCF), UMR 6296 Université Clermont Auvergne, CNRS, SIGMA Clermont, 63000, Clermont-Ferrand, France

[4] Institute of Biomaterials, Department of Materials Science and Engineering, University of Erlangen-Nuremberg, 91058, Erlangen, Germany

[5] Institute of Polymer Materials, Department of Materials Science and Engineering, University of Erlangen-Nuremberg, 91058, Erlangen, Germany

[6] Centre Imagerie Cellulaire Santé (CICS), UCA PARTNER, 63000, Clermont-Ferrand, France

[7] Mines Saint-Etienne, Univ Lyon, CNRS, UMR 5307 LGF, Centre SPIN, F - 42023 Saint-Etienne France

[8] Mines Saint-Etienne, Univ Lyon, CNRS, Univ Jean Monnet, Univ Lumière Lyon 2, Univ Lyon 3 Jean Moulin, ENS Lyon, ENTPE, ENSA Lyon, UMR 5600 EVS, Centre SPIN, F - 42023 Saint-Etienne France

*** Corresponding author**

Lukas Gritsch, e-mail: lukas.gritsch@clermont.in2p3.fr

Laboratoire de Physique de Clermont, UMR CNRS 6533
Université Clermont Auvergne
4 avenue Blaise Pascal
63178 Aubière
France

Abstract

Recently, additive manufacturing became the subject of intense study in biomaterials science. Thanks to their versatility and effectiveness, this family of processing techniques could completely revolutionize the field. In bone regenerative medicine, in particular, additive manufacturing seems incredibly promising in opening new avenues of development of patient-specific *ad hoc* therapies. They could make possible to scan a defect and precisely replicate it to offer the best fitting for each patient. The main bottleneck to date is the relatively scarce availability of materials that can be printed reliably and consistently. This is the case for organic/inorganic hybrids, materials produced by sol-gel chemistry that combine the advantages of polymers and bioinorganics at the molecular scale. Due to their complex structure and unique rheological and mechanical properties, the printing of hybrids remains challenging. With this study, we aim to investigate the rheological, thermal and molecular properties of a class I polycaprolactone/bioactive glass hybrid and discover how they relate to the printability of the material. The molecular weight distribution (gel permeation chromatography), thermal properties (thermal gravimetric analysis, differential scanning calorimetry) and rheological properties of each hybrid material were investigated at all stages of processing. Printing trials via direct fused deposition modeling were performed on all polymers as received and on their respective hybrids. Morphological characterization of the printed constructs was also performed. Finally, their apatite forming ability in simulated body fluid was evaluated by scanning electron microscopy and particle-induced X-ray emission. Results confirmed the successful direct 3D printing of organic/inorganic hybrids for the first time. Three-dimensional scaffolds were successfully produced without the need for additional solvents or indirect approaches. Thanks to the thermal analysis, an ideal temperature window for printing was identified. SBF immersion assays confirmed that the material's bioactivity is retained after printing. Thanks to our findings, fused deposition modeling might develop into a suitable technique for fabricating 3D bioactive scaffolds for bone tissue engineering.

1 Introduction

Processing biomaterials using additive manufacturing (AM) is a rapidly expanding topic, captivating the interest of researchers worldwide for its versatility and reproducibility. AM methods, also commonly referred to as 3D printing, indicate a group of fabrication techniques used to create layer-by-layer structures from a computer-aided design (CAD). Some AM processes include stereolithography, fused deposition modeling (FDM), or 3D bioplotting. They offer highly customizable solutions to the fabrication of 3D structures with precise tailoring of porosity and mechanical properties. These key advantages make them very promising strategies to design and develop the next generation of scaffolds for tissue repair, tissue engineering and other biomedical applications in general[1,2]. The development of 3D constructs using AM could be a particularly promising strategy for patient-specific therapies and *ad hoc* clinical approaches, especially in orthopedics and bone regenerative medicine. Currently, the main limitations for the successful application and industrialization of 3D printing techniques consist mainly in the relatively high limits of resolution (i.e., limited to the microscale, while cells and tissue are highly susceptible to nanotopography) and the scarce availability of materials that combine reliable printability with competitive biological performance. The primary printed materials currently under investigation for bone tissue engineering are calcium phosphates, such as hydroxyapatites (HA) and tricalcium phosphates (TCP), often combined with polymers. Some notable examples are various types of polyesters (polylactic acid, polyglycolic acid, polycaprolactone), methacrylates (e.g., poly(ethylene glycol) dimethacrylate, PEGDMA) and natural polymers (collagen, alginate, gelatin)[3,4]. These materials are mostly used as components of conventional composites, with several intrinsic drawbacks and limitations, especially in terms of resolution and integrity of the matrix/filler interface[5]. Born with the goal of overcoming the limits of conventional composites, sol-gel organic/inorganic (O/I) hybrids are a family of materials with unique physical and biological properties. They are usually defined as a single-phase network of two or more components (both organic and inorganic) combined at the molecular level by sol-gel chemistry-based synthesis procedures[6]. Typically, O/I hybrids are described depending on their organic-inorganic interactions and organized into five classes accordingly: with weak interactions such as hydrogen bonding, molecular entanglement, or van der Waals forces (class I), with covalent bonding between organic and inorganic chains (class II), with weak interactions but prepared by a one-pot synthesis with two monomeric precursors (class III), one-pot synthesis with O/I covalent bonds (class IV) and finally with weak interactions from one single O/I precursor (class V)[7]. Scientific literature offers a wide selection of hybrid formulations prepared using various polymers and several inorganic candidate compositions. In biomedical applications, most studies focus on silicate-based inorganic components, although borate-based are also explored with promising results. A source of calcium is also often added to increase bioactivity, that is, its ability to trigger and/or enhance the formation of apatite crystals once introduced in a physiological-like environment. A significant number of candidate polymers is also reported. Synthetic polymers such as polycaprolactone, polymethylmethacrylate, poly(tetramethylene succinate) or polydimethylsiloxane showed promising processing characteristics, mechanical properties and biological performance[6]. Naturally sourced materials (i.e., gelatin[8–10], chitosan[11,12], alginate[13] or γ-polyglutamic acid[14]) are also interesting options, in particular for their ability to have significant effects on cell behavior and to be used as carriers for therapeutic ions, especially calcium. These hybrid materials are typically characterized by a remarkable performance for their application in bone and cartilage regeneration, with ideal mechanical properties for the purpose and an unmatched ability to stimulate bone mineralization and cell differentiation.

Given how these materials could have a disruptive impact on bone and cartilage tissue engineering, efforts have been made to 3D print O/I hybrids. Additive manufacturing techniques could highly improve the current status in hybrids scaffold fabrication, mostly bound to techniques that render poorly controllable geometries and topographies, such as solvent casting/particulate leaching[15,16] or electrospinning[17,18].

To date, achieving reliable and reproducible 3D printing of an O/I hybrid material remains an open challenge. There are several possibilities currently under investigation. Tallia *et al.*[19], for instance, reported direct sol printing of class II/IV hybrid of polycaprolactone (PCL), silica and poly(tetrahydrofuran): 3D structures are prepared using the material while still in its sol state before the condensation of the silica network. This approach results in three-dimensional scaffolds with 200 μm pores for cell infiltration, a unique bouncing mechanical behavior and self-healing properties. However, direct sol printing poses significant drawbacks in terms of scalability due to the ever-evolving rheological properties of the sol-gel mixture and the limited timeframe available for printing before gelation occurs. Another possible approach is to use UV-based techniques. For instance, a silica-based hybrid system prepared from tetramethylorthosilicate (TMOS), trimetoxymethylsilane (MTMS) and 3-acryloxypropyltrimethoxysilane (APTMS)[20]. The scaffolds prepared with this technique have excellent mechanical properties, high stability and remarkable transparency (89 %). The organic content, however, is minimal and it is limited to the sole coupling agent (APTMS). For this reason, the definition of the material as a "hybrid" could be questioned. In addition, the material was not specifically developed for biomedical purposes and, as a consequence, it has the disadvantage of being too inert (no bioactivity) and rigid for most applications in contact with the organism. The authors foresee its use in the production of microfluidic reactors and molds for the dental industry. One of the most scalable and promising AM-based methods to fabricate hybrid scaffolds for tissue engineering was recently proposed by Hendrikx *et al.*[21], expanding from more traditional protocols that explored the use of sacrificial templating in conjunction with sol-gel hybrids (see, for instance, the use of polymeric microspheres). The authors developed an indirect rapid prototyping method combining FDM and sacrificial template solvent leaching. Briefly, a wood-pile polymeric structure was first printed with PCL, then infiltrated with a class II PEO/silica hybrid sol and finally, after complete gelation, the PCL template was dissolved using an appropriate solvent (tetrahydrofuran). This approach by-passes the intrinsic difficulties related to direct hybrid printing and focuses the AM process on the much more reliable PCL. Structures resulting from this fabrication procedure, negatives of the originally printed template, are highly interconnected 3D hybrid scaffolds with a topography that can be finely tailored by varying FDM parameters. Other promising advantages of the method include (i) the ability to enhance apatite formation already after 7 days of immersion in physiological-like fluids, (ii) ideal biocompatibility (using a SaOS-2 cell line) and (iii) adequate mechanical properties for bone regeneration applications. Nevertheless, the technique remains characterized by important drawbacks: it is highly time and material consuming and consumes significant quantities of solvents for complete template leaching. A solution to retrieve sacrificial PCL should also envisaged to avoid additional waste. These characteristics limit the scalability of this methodology.

Although current findings on O/I hybrid printing are promising, direct hybrid FDM could be a game changer. It could offer a very standardized, scalable and reproducible method without the need for high quantities of material and solvents. It could also avoid the intrinsic time limitation of techniques that exploit the sol phase of hybrids. In addition, compared to solvent-based solutions, thermal-based processing techniques such as FDM offer highly

increased mechanical properties. Crucial open challenges are the difficulty in identifying adequate printing parameters and the possible thermal degradation related to the necessary high temperatures.

To our knowledge, no direct FDM of O/I hybrids is reported to date, in spite of the possible advantages of the method over other AM procedures. For this reason, in this study we explored the subject and led an investigation into the printability of O/I hybrids using a previously reported class I PCL/bioactive glass (BG) hybrid that already showed outstanding physicomechanical and biological performances. The study had three main goals: (i) characterize the printability of PCL/BG hybrids as a function of polymer characteristics, (ii) identify printing parameters and relevant characterization methods to predict printability and (iii) verify that once printed hybrids retain their ability to leach therapeutic ions and help the formation of apatite (bioactivity). Printed samples were subject to an in-depth thermophysical characterization by thermogravimetric analysis (TGA), gel permeation chromatography (GPC), rheology and differential scanning calorimetry (DSC). The stability and bioactivity in simulated body fluid (SBF) were also assessed by scanning electron microscopy (SEM), inductively coupled plasma-atomic emission spectroscopy (ICP-AES) and particle-induced X-ray emission (PIXE).

2 Materials & Methods

2.1 Polycaprolactone/bioactive glass hybrids synthesis

Polycaprolactone (PCL) and silica/calcium binary bioactive glass (BG) were combined into class I hybrids adapting a previously reported sol-gel method carried out at room temperature[15,16]. The theoretical organic/inorganic weight ratio was 70:30. Similar sol-gel synthesis procedures were repeated changing the selected polycaprolactone, investigating how variations in polymer selection could ultimately influence the 3D printability and the overall properties of the material. Three PCLs (Purasorb® PC08, PC12 and PC17, Corbion) with an inherent viscosity of 0.8 g/dL, 1.2 g/dL and 1.7 g/dL, respectively, were selected among other candidate materials. Inherent viscosity is known to be proportional to the molecular weight of a polymer following the Mark-Houwink equation[22]:

$$\eta = K \cdot MW^{\alpha}$$

Where η is the inherent viscosity, MW the molecular weight and K and α are two empirical coefficients. The hypothesis is that by varying this parameter it is possible to tailor the rheological properties of the hybrid and, therefore, its printing behavior.

In a typical synthesis process, tetraethyl orthosilicate (TEOS, 99 % purity, Sigma-Aldrich) is initially hydrolyzed for 30 minutes in a chosen volume of absolute ethanol (Sigma-Aldrich) and 2M HCl (obtained diluting 37 % fuming HCl, Sigma-Aldrich, in deionized water). The molar ratio of the ethanol/H_2O/TEOS/HCl mixture is 3.7:2:1:0.07. Calcium hydroxide ($Ca(OH)_2$, 98 % purity, Acros Organics) is then suspended in an equal volume of absolute ethanol and added to hydrolyzed TEOS. Catalyzed by the increase in pH caused by $Ca(OH)_2$, the condensation of the silica network initiates, ultimately leading to the gelation of the inorganic sol. The quantity of calcium source is adjusted to obtain a final composition of 75 wt.% SiO_2 - 25 wt.% CaO, chosen for its rapid apatite forming ability[23]. In parallel, PCL is dissolved in tetrahydrofuran (20 % w/v). Before the complete gelation of the SiO_2-CaO mixture, the BG sol is mechanically mixed with the organic solution, sonicated for 1 hour, aged at room temperature for varying periods (1h or 24h, see later) and finally cast into glass petri-dishes to air dry. The

final material is milled to a coarse powder (IKA A11 basic analytical mill) and stored under vacuum at -18 °C until further processing.

2.2 Hybrids fused deposition modeling and analysis of printability

The three PCLs and their respective hybrids were employed to fabricate scaffolds by fused deposition modeling (FDM) using a BioScaffolder 3.2 (GeSiM mbH) equipped with a high-temperature mechanical extrusion module (HT-extruder, 500 µm nozzle, GeSiM mbH). The printing conditions were adapted according to tested material, extrusion speed and temperature. The Bioscaffolder grants independent temperature control over the cartridge and the nozzle, the later being usually hotter due to the gradually reduced volume within the conical tip, requiring an increased fluidity of the molten material. Parameters as a function of the PCL or hybrid are reported in Table 1. Several combinations were tested following a trial-and-error approach and varying cartridge and nozzle temperatures in the 50-120 °C range, as well as feed from 1 to 20 µm/s. The printing speed was not an independent variable and it was generally adjusted according to the feed and the printed material. The material was heated inside the extrusion syringe for one hour before printing. Cylindrical scaffolds (Ø=10 mm and thickness=10 mm) with 1, 3, 5, or 7 struts per layer (20 layers in total) were printed for morphological analysis and printability assessments. Thinner 3-layered scaffolds (Ø=10 mm, 5 struts per layer) were instead prepared for all other characterizations.

Table 1: Key printing parameters. Note how higher inherent viscosity results in higher nozzle printing temperatures and lower printing speed. Similarly, hybrids need higher temperatures and lower speeds than their native polymer.

Material	Cartridge temperature (°C)	Nozzle temperature (°C)	Feed (µm/s)	Speed (mm/s)
PC08	*60*	*62*	*8*	*10*
PC12	*60*	*67*	*6*	*8*
PC17	*60*	*75*	*4*	*6*
HPC08	*70*	*82*	*3*	*4*
HPC12	*70*	*87*	*3*	*4*
HPC18	*70*	*95*	*2*	*3*

2.3 Thermal and physical analysis

2.3.1 Thermal gravimetric analysis

The thermal behavior and degradation of all materials was studied by thermogravimetric analysis (TGA) using a 550 Discovery Series (TA Instruments, USA). A standard 10 mg sample was heated from room temperature (circa 20°C) to 800 °C at 10 °C/min in nitrogen atmosphere, measuring weight variation as a function of temperature.

2.3.2 Gel permeation chromatography

The molecular weight distribution and polydispersity (PD) of the three PCLs and their respective hybrids before and after printing (12 samples in total) were measured by gel permeation chromatography (GPC). The analysis was performed to identify possible damages caused by the alkalinity of the synthesis environment and/or the thermal stress induced by FDM. Materials were dissolved in Hexafluoroisopropanol (HFIP) at a concentration of 8 g/L and syringe filtered. Following this step, the percentage recovery of material was calculated. Calibration was performed using 60 kDa polymethylmethacrylate (PMMA) with narrow molecular weight distribution. The testing

setup was composed of a Viscotek TDA 305 GPC/SEC detector module (Malvern Instruments) equipped with a Viscotek GPCmax solvent and sample delivery module (Malvern instruments) and a PFG analytical column (PSS). The analysis was performed at 35 °C at 0.8 ml/min flowrate. As determined in previous experiments, the refractive index increment used was 0.1854 cm3/g. Data were recorded and computed by OmniSEC 4.70 (Malvern Instruments). The recorded parameters were number average molecular weight (Mn), mass-average molecular weight based on average weight (Mw) and polydispersity (PD = Mw/Mn).

2.3.3 Rheology

Rheological analysis using an ARES rheometer (TA Instruments, USA) was performed to characterize the behavior of hybrids as a function of the printing temperature, the duration of aging and the chosen polymer. Nine materials were tested in total: the three PCLs as-is, PCL-based hybrids prepared as described above (HPC08, HPC12 and HPC17) without (n) and with (w) the prolonged 24h aging step. Frequency sweep tests (0.1 – 100 rad/s) were performed within the linear viscoelastic (LVR) region of the materials. Samples of all polymers and their respective hybrids were tested using parallel plates (Ø = 10 mm) at their respective printing temperatures. Testing temperature and strain for each material are reported in Table 2. Average coefficients indicating the proportional increase in viscosity for both short (I_N) and long (I_W) aging were also defined as follows:

$$I = \frac{1}{n}\sum_{i=1}^{n}\frac{\eta^*_{HPC}(f_i)}{\eta^*_{PC}(f_i)}$$

Where $\eta^*_{HPC}(f_i)$ and $\eta^*_{PC}(f_i)$ are the values of complex viscosity at a given frequency f_i for each hybrid (with longer aging for the calculation of I_W, shorter for the calculation of I_N) and its respective native polymer.

Table 2: Summary of samples tested by frequency sweep.

Material	Aging Time	Temperature (°C)	Strain (%)
PC08	N/A	*62*	*10*
PC12		*67*	
PC17		*75*	
n-HPC08	1 h	*82*	*2*
n-HPC12		*87*	
n-HPC17		*95*	
w-HPC08	24 h	*82*	*0.03*
w-HPC12		*87*	
w-HPC17		*95*	

Temperature ramp tests were also performed to investigate the effect of temperature variations on the rheological behavior of PCL/BG hybrids. The samples were subject to a 5 °C/min ramp from 50 to 160 °C at 1 rad/s and 5 % (PCLs) or 2% strain (hybrids).

2.3.4 Differential scanning calorimetry

Differential scanning calorimetry (DSC) measurements of the various PCLs and their respective hybrids in 10 mg aliquots were performed using a Q2000 (TA Instruments, USA). Dynamic heating experiments were conducted at a 10°C/min ramp from -75°C to 200°C over two heating cycles (H1 and H2, respectively). All tests were conducted under a dry nitrogen flow of 20 mL/min and repeated three times. DSC was used to evaluate possible variations

in the degree of crystallinity of PCL upon hybrid synthesis. The degree of crystallinity χ was calculated using the formula:

$$\chi = \frac{\Delta H_m - \cancel{\Delta H_c}}{\Delta H_m^\circ} \quad \rightarrow \quad \chi = \frac{\Delta H_m}{\Delta H_m^\circ}$$

Where ΔH_m is the measured enthalpy of melting (integral of the melting peak in time), ΔH_c the enthalpy of crystallization during the heating cycle (zero for the PCL here used) and $\Delta H°_m$ is the standard enthalpy of melting of 100 % crystalline PCL, according to literature equal to $\Delta H°_m$ (PCL) = 136 J/g[24,25]. Since the PCL here employed is not characterized by a crystallization peak during heating ($\Delta H_c = 0$) – meaning the PCL used were already at maximum degree of crystallinity when starting the DSC measurement, the formula is simplified as shown above.

2.4 Degradation and bioactivity

2.4.1 Monitoring of stability in simulated body fluid

Stability (pH, weight loss) and apatite-forming ability tests were performed using simulated body fluid (SBF) as model fluid. SBF was prepared according to the protocol published by Bohner and Lemaitre[26] and stored in plastic bottles for a maximum of 30 days. Scaffolds for testing (n = 5) were immersed in SBF at a 1.5 mg·mL−1 ratio, as suggested by the unified in vitro evaluation protocol for apatite-forming ability by Maçon et al.[27] and incubated under agitation (250 rpm) at 37°C. At selected time points (1, 3, 7, 14 and 21 days), samples were rinsed in deionized water first and ethanol second, air dried and finally weighted. In parallel, the pH and ion concentration of the solutions were measured. The concentration of Ca, P and Si ions was determined using Inductively Coupled Plasma-Atomic Emission Spectroscopy (ICP-AES).

2.4.3 Scanning electron microscopy

Morphological analysis of the 3D structure of the printed scaffolds and a first qualitative assessment of the apatite formation on the surface of the samples was performed by scanning electron microscopy (SEM) using a Regulus 8230 Field Emission Gun Scanning Electron Microscopy (FEG-SEM, Hitachi). Prior to analysis, the samples were sputter coated with carbon (Emitech E6500, Quorum). In parallel, Energy-Dispersive X-ray spectroscopy (EDX) was used to confirm the presence of calcium and phosphorus in the samples. Punctual and cumulative spectra were acquired from various samples at multiple positions using a Silicon Drift Detector (SDD) X-MaxN, Oxford Instruments, UK.

2.4.4 Particle-induced X-ray emission

After immersion in SBF, samples were also analyzed with a Particle-Induced X-ray Emission (PIXE) nuclear microprobe. Similar to Energy-Dispersive X-ray spectroscopy (EDX), but with 100 times the sensitivity[28], PIXE is an elemental analysis that can be used to map the presence of desired elements (i.e., Si, Ca,P) inside the material in order to get a more quantitative assessment of the bioactivity of 3D printed PCL/BG hybrids. At each SBF immersion period, reacted scaffolds of all typologies were embedded in epoxy resin (Agar 100 Resin, agar scientific) and cut into thin slices using a low speed diamond saw (thickness=150 µm). Quantitative chemical imaging of the samples was performed in collaboration with the AIFIRA platform (CENBG, France) using a 3 MeV incident proton beam (beam diameter=1 µm). X-ray detection was carried out with an 80 mm^2 Si(Li) detector equipped with a 12 µm-thick beryllium window and a 100 µm aluminum funny filter (central hole diameter=2 mm, tilted 135° with respect to the incident beam axis). The Gupixwin software was used to determine the

concentrations of Si, Ca and P ions within the sample. A soda-lime glass (NIST-620) was used as standard reference material for the calibration of the machine.

3 Results and discussion

3.1 Chemical, thermomechanical and rheological material analysis

3.1.1 TGA

A comprehensive analysis of the thermal and mechanical properties of the selected PCLs (TGA, DSC, rheology and GPC) and their respective hybrids was performed to characterize their behavior and identify the key variables that could make PCL/BG hybrids consistently 3D printable. TGA results showed single-stage weight loss for all samples (Figure 1). No substantial difference in degradation rate was observed between PCL samples. Curves for PC08, PC12 and PC17 are almost identical. All three PCLs, in particular, are characterized by the typical decomposition step of the polymer at around 410 °C. A minor indentation can be observed at a slightly lower temperature (~360 °C), especially on PC08 and PC12. This is also reported in literature and can be better measured using high-resolution TGA techniques[29].

Table 3: Thermal properties of PCL and its hybrids from TGA measurements.

	Onset of weight loss (°C)	Degradation peak (°C)	Final inorganic component
PC08	*360*	*410*	*0.2 %*
PC12	*360*	*410*	*0.3 %*
PC17	*360*	*410*	*-11.8 %*
HPC08	*330*	*390*	*23.5 %*
HPC12	*320*	*385*	*25.0 %*
HPC17	*320*	*395*	*26.8 %*

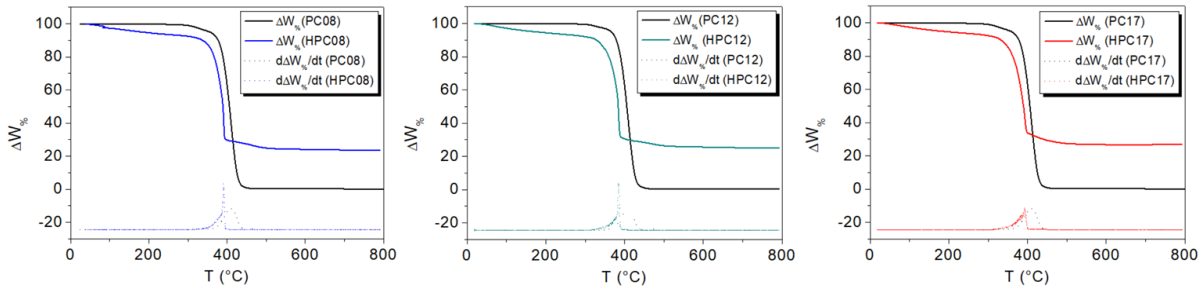

Figure 1: ΔW% and d ΔW%/dT from 20 °C to 800 °C for PC08 (left), PC12 (middle) and PC17 (right) and their respective binary hybrids

Briefly, the thermal degradation of PCL can be described as a two-stage mechanism. The first stage INDICATE TEMPERATURE is characterized by a statistical rupture of the polyester chains via ester pyrolysis. The reaction produces H_2O, CO_2 and 5-hexenoic acid, all released as gas. The second step INDICATE TEMPERATURE leads to the formation of the cyclic monomer of PCL, ε-caprolactone, via unzipping depolymerization[29]. Only minor variations to this trend occur in the case of hybrid samples. They are characterized by a slight decrease in degradation on-set temperature and by a minor ramp of initial weight loss starting at T<100°C. This is probably associated with the solvent evaporation (EtOH, THF) and possibly the condensation of remaining precursors (i.e., silanols) from the sol-gel synthesis, as suggested in previous similar studies[30,31]. The decrease could also be associated with solvent evaporation[32]. The final residual weight of the three polymers were 0.2 % (PC08), 0.3 % (PC12) and 0.2 % (PC17), respectively (Table 4). PCL is expected to leave a negligible residue after TGA, as confirmed by literature on the topic[29,30]. The inorganic weight residues for hybrids are 23.5 % (HPC08), 25.0 % (HPC12) and 26.8 % (HPC17), respectively (Table 4). These values are consistent with the theoretical inorganic content (i.e., 25 %).

3.1.2 GPC

GPC was carried out to investigate possible effects of sol-gel synthesis and 3D printing on the original MW of the three PCLs used. The effect of sol-gel hybrid synthesis on the analysis is first observed as a significant decrease in solubility: recovery drops from 100 % to about 65 % (for more details, see supplementary data). This value confirms good recovery efficiency. Silica nanoparticles are not soluble in HFIP, while PCL can be resolubilized and recovered. Since the nominal ratio of the polymer is 70 %, it can be concluded that most of the polymer inside the hybrid can be successfully recovered and analyzed. No significant variation in recovery was observed in printed materials. PC08, PC12 and PC17 have typical distributions for PCL, with a number average molecular weight (Mn) of circa 20, 35 and 60 kDa, respectively. The weight average MWs (Mw), were instead circa 40, 60 and 100 kDa, respectively. As expected, values increase according to their inherent viscosity (Table 4). Polydispersity (PD) is uniform across polymer type (~ 1.8). The analysis of recovered PCLs highlighted the occurrence of a minor decrease of MW coupled with a slight widening of the distribution in the case of PC08 (Table 4). The reduction can be ascribed to the breaking of ester bonds due to alkaline hydrolysis. The reaction is catalyzed by the high pH of the synthesis pot, necessary for the successful gelation of the silica network. Reductions in MW and widening of the MW distribution were also identified following 3D printing for all PCLs, probably because of thermally induced chain breakage. On the contrary, absence of relevant variations in the MW distributions was observed for hybrid samples. The case of printed HPC12 is particularly remarkable, characterized even by a slight increase of both Mw and Mn, coupled with no variation in polydispersity.

Table 4: Results of GPC for all tested PCLs and hybrids before and after printing. Percentage variations with respect to a relevant control are also shown. The control is the same material before the processing under consideration (i.e., PCL in the case of hybrids before printing and PCL after printing, hybrids before printing in the case of hybrids after printing).

Material	*Before printing*			*After printing*		
	Mw (kg/mol)	**Mn (kg/mol)**	**PD**	**Mw (kg/mol)**	**Mn (kg/mol)**	**PD**
PC08	43.2 ± 1.0 -	23.7 ± 1.8 -	1.8 -	41.7 ± 0.2 *- 3.5 %*	21.1 ± 1.3 *- 10.9 %*	2.0 *+ 11.1 %*
PC12	61.0 ± 0.3 -	34.6 ± 0.7 -	1.8 -	60.8 ± 0.3 *- 0.3 %*	30.2 ± 0.3 *- 12.7 %*	2.0 *+ 11.1 %*
PC17	101.8 ± 0.3 -	60.1 ± 2.6 -	1.7 -	92.5 ± 1.0 *- 9.1 %*	57.5 ± 2.3 *- 4.3 %*	1.6 *- 5.9 %*

HPC08	41.2 ± 0.4	*- 4.6 %*	16.2 ± 0.7	*- 31.6 %*	2.5	*+ 38.9 %*	39.4 ± 0.5	*- 4.4 %*	18.9 ± 0.7	*+ 10.7 %*	2.1	*+ 16.0 %*
HPC12	60.4 ± 0.4	*- 1.0 %*	33.8 ± 1.5	*- 2.3 %*	1.8	*0 %*	63.2 ± 0.9	*+ 4.6 %*	35.9 ± 1.6	*+ 6.2 %*	1.8	*0 %*
HPC17	97.8 ± 1.9	*- 3.9 %*	58.8 ± 1.5	*- 2.2 %*	1.7	*0 %*	98.7 ± 1.7	*+ 0.9 %*	56.2 ± 1.9	*- 4.4 %*	1.8	*+ 5.6 %*

These findings suggest that hybrids are more stable against the stress imposed during printing than PCL used alone. Generally speaking, the alterations in MW observed with GPC are acceptable and confirm that both the sol-gel synthesis protocol and the FDM process do not pose an excessive source of degradation for the polymer. Among a choice of different PCLs, higher MW polymers should be preferred over lower MW ones: they were found to be more resistant to the alkaline environment necessary for the sol-gel hybrid synthesis. However, as mentioned above, there is a close relationship between chain length and polymer viscosity. Although it can protect the material from premature degradation, the MW of the source PCL cannot be increased indefinitely without significantly affecting the viscosity and the overall flow behavior of hybrids. This consideration led us to look into the rheology of PCL/BG hybrids.

3.1.3 Rheology

The rheological properties of fused PCLs and its hybrids can shed a light on several key variables contributing to the successful 3D printing of these materials. Investigations were carried out to characterize the rheological behavior as a function of frequency and temperature. All tests were performed within the LVR. The range was found to widen the lower MW of PCL. More interestingly, a significant ten-fold decrease of LVR was observed for hybrids compared to their respective PCL (Figure 2). THE LVR IS USUALLY DETERMINED BY PLOTTING G' AND G'' AGAINST THE STRAIN γ, NOT THE FREQUENCY. THEREFORE I DON'T UNDERSTAND WHY THE LVR WOULD BE VISIBLE ON FIG 2?

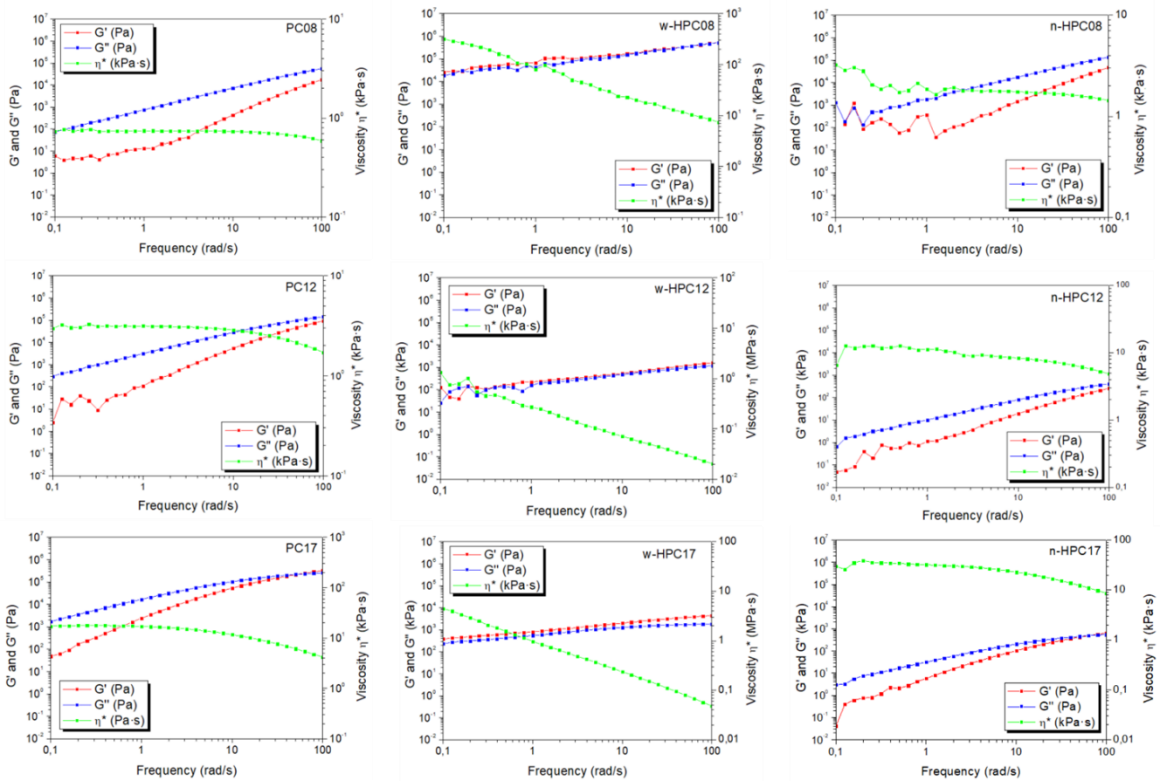

Figure 2: G', G'' and η* for all PCLs (left), 24h-aged hybrids (middle) and 1h-aged hybrids (right). PC08, PC12 and PC17 as a function of frequency. In the case of 24 h aging, note that (1) viscosity increases circa three order of magnitude from a PCL to its hybrid, from kPa to MPa, (2) there are significant variations in how viscosity changes as a function of frequency, compared to the pure polymer. With 1 h aging hybrids retain the native rheological behavior of their respective PCL with only a minor increase in the absolute value of viscosity. The materials were heated during the experiments (see Table 2 for detailed conditions).

The reduction can be controlled by tailoring the length of the aging step. Frequency sweep results carried out at target printing temperatures confirmed the characteristic shear thinning behavior of PCL for all tested polymers[33–36]: viscosity decreases for higher frequencies of deformation. In particular, in PC08 and PC12 samples, viscous behavior is predominant over elastic one (G'' > G'). On the contrary, PC17 has a crossover gel point at between 40 and 50 rad/s. The gel point is shifted towards lower frenquencies with increasing MW, meaning the domain where the viscous behaviour is predominant is reduced when MW is increased. The original rheological behavior of PCL significantly changes after synthesis. The nature of the change is very different depending on the occurrence/lack of an aging step. Without aging, the hybrids preserve the rheological trends of their respective PCL (G', G'' and viscosity) but with a two-fold increase. The crossover point of PC17 increases to 60 rad/s. These results are consistent with previous reports on similar materials[37]. If 24 hours of aging is applied, all hybrids show a solid-like behavior (G' > G'') with highly increased shear thinning. Finding a suitable feed for the 3D printing of aged hybrids appears to be challenging. The coefficients I_N and I_W (see definition in Mat & Methods section) established to quantify the variations in viscosity with and without aging confirm this hypothesis (Table 5).

Table 5: Coefficients associating the viscosity trend of tested PCLs with their respective O/I hybrids with 1 h (I_N) or 24 h (I_W) aging, as measured by rheology.

Starting polymer	I_N	I_W
PC08	1	7
PC12	2	11
PC17	2	16

No significant change was assessed between PC08 and n-HPC08. The viscosity of PC12 and PC17 instead doubles after synthesis. With 24 h of aging, the changes in viscosity are more sizeable and highly frequency dependent. That is, for low frequencies the values of viscosity skyrocket to several hundred times the one of PCL. The increase in viscosity is strongly associated with the increase of MW (see GPC analysis). For higher frequencies (> 10 rad/s), the viscosity trend is comparable between hybrids and their respective polymer. Also here, the increase is greater for polymers of higher MW. The correlation between MW and viscosity variation could be explained as a consequence of the synthesis. In particular, polymers with lower MW tend to have low viscosity in THF and do not match the viscosity of the BG sol, causing phase separation and ultimately producing a less entangled structure that retains the properties of the original polymer. In light of these findings, using a mid-MW PCL with a short aging step seems to be favorable for obtaining a more homogeneous hybrid material with fluid-like behavior at low viscosity. Adapting the synthesis protocol with particular attention to this step (i.e., decreasing the aging time) is an effective approach to optimize the rheological properties of O/I hybrids for the best possible printability in 3D. One-hour aging compromises the development and interconnection of the silicate network in favour of the printability. In other words, shorter aging allows for the formation of a less interconnected inorganic network and, as a consequence, the final material retains the native rheological properties of PCL.

In addition to frequency sweep (

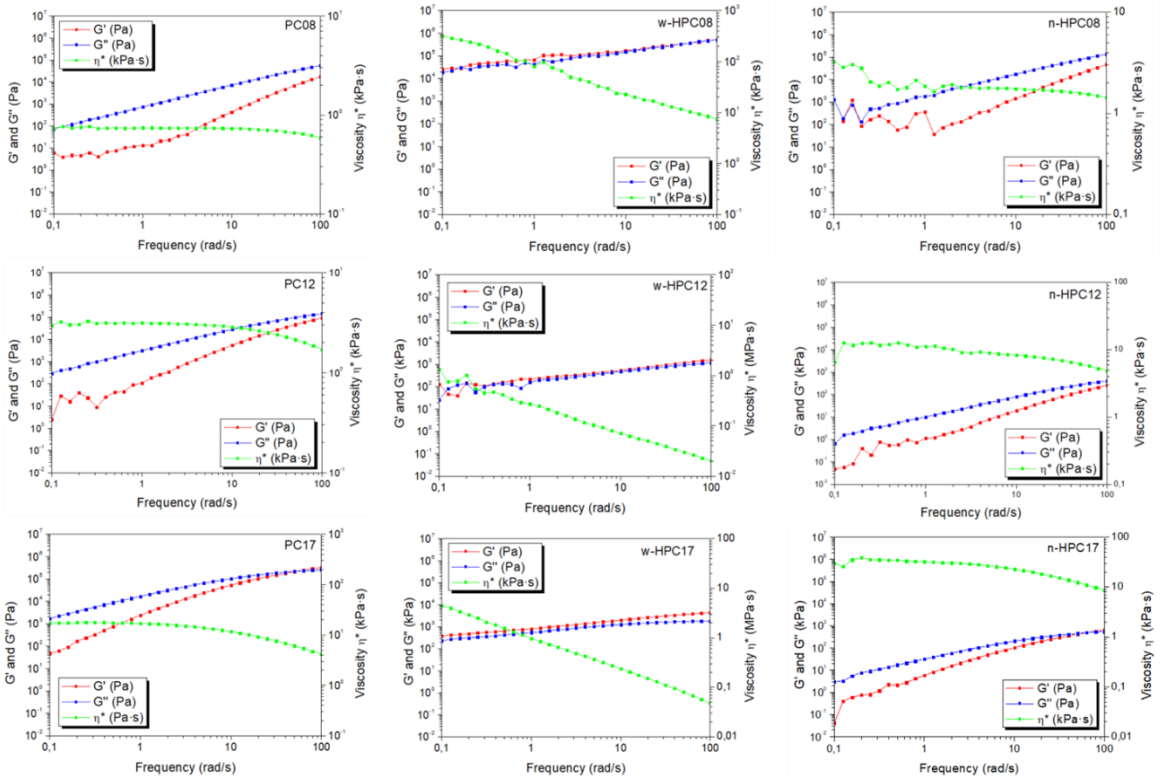

Figure **2**), the variation of viscosity as a function of temperature was investigated between 50 °C and 160 °C on the more promising hybrid candidates (1h aging, for their more controllable rheological properties) and their respective PCLs. Initial trial-and-error prototyping experiments highlighted the key importance of temperature for the successful 3D printing of PCL/BG hybrids. In particular, temperatures above 100 °C led to irreversible nozzle clogging and failure to print. The results of rheology further supported these findings. As expected for all materials, the viscosity decreases with increasing temperature. The hybrids follow a similar trend, however at increased viscosity levels, as already observed with frequency sweep measurements. Most remarkably, all three hybrids present a major peak formation at around 120-130 °C. Above 130 °C, viscosity follows an increased linear trend. This result is most probably ascribed to further condensation of residual silanols after synthesis. Catalyzed by temperature, free Si-OH moieties covalently bond seem to boost network connectivity and, ultimately, determine an increase in viscosity that hinders the reproducibility of 3D printing above 100 °C.

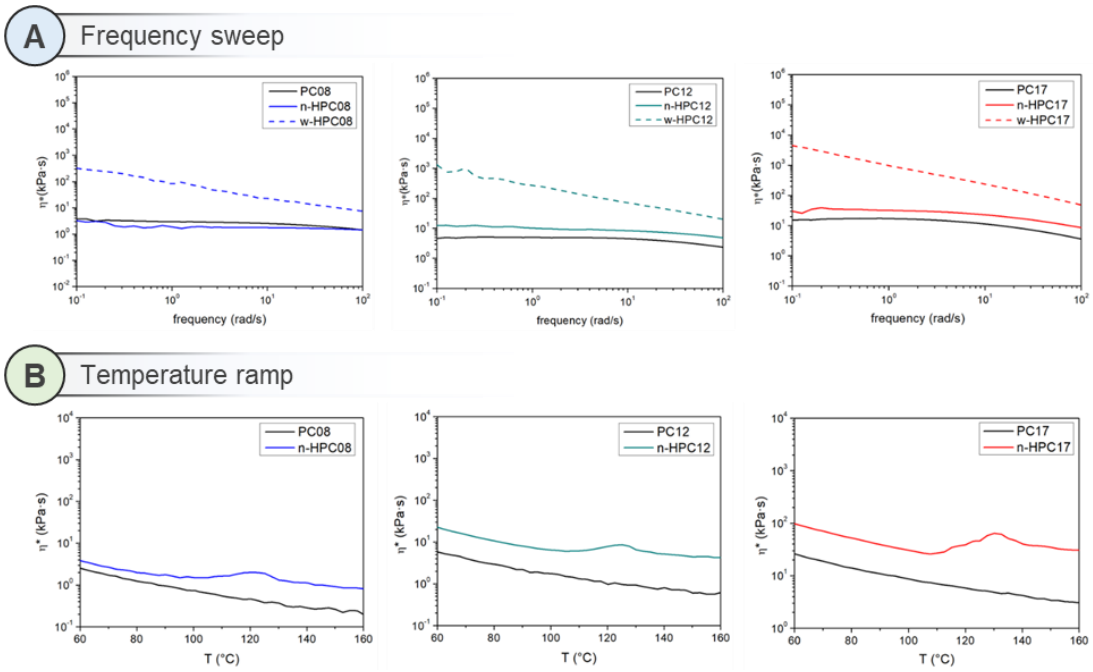

Figure 3: (A) Comparison of complex viscosity as a function of frequency for tested PCLs and their respective hybrids. The materials were heated during the experiments (see Table 2 for detailed conditions). (B) Temperature ramps showing the occurrence of a significant increase in viscosity at 120 °C following hybrid synthesis (with 1h aging). This phenomenon explains the lack of reproducibility of printing above 100 °C.

3.1.4 DSC

Expanding on the findings of rheology, DSC was performed to confirm the identification of the temperature range of interest to print without significant damage to the hybrid. Table 6 summarizes the key DSC parameters for all tested materials. In agreement with previous reports on the topic[38,39], the DSC of PC08, PC12 and PC17 were characterized by three areas of interest: (i) a small shoulder around -60 °C degrees corresponding to the glass transition temperature (T_g) of PCL, (ii) an endothermic peak at 60 °C appearing during heating cycles caused by the melting of the polymer and (iii) an exothermic peak during cooling due to PCL recrystallization AND iv) 2ND ENDOTHERMIC PEAK FOR HYBRIDS (at 120-150°C)? A slight decrease in intensity of the peaks can be observed for PCLs with higher MW, probably as a consequence of different folding mechanisms of the polymeric chains depending on their molecular hindrance[40]. Printing has no significant effect on PCL, owing to the relatively low temperature at which it is performed. The most remarkable difference is a shift of the recrystallization peak towards higher temperatures. Pre-printing cold crystallization occurs at relatively low temperatures compared to other studies[41], probably due to the high cooling rate used (i.e., -10 °C/min)[42]. After printing, a shift towards higher temperatures is observed. However, hybrid synthesis does not cause substantial variations compared to PCL characteristic peaks. This confirms previous results indicating that the synthesis procedure does not significantly alter the native properties of the polymer. The hybrid printing process does not determine significant variations either. Interestingly, the previously observed shift in the crystallization peak is completely absent when analyzing hybrid samples. It could be that the interpenetrated silica network hinders further crystallization. Conversely, printing determines a slight asymmetry in the melting peak of first heating (H1). This difference is lost on second heating (H2).

Table 6: Relevant thermal parameters of all PCLs and hybrids as measured by DSC.

Material	T_g (°C)	T_{CC} (°C)	ΔH_{CC} (J/g)	T_m (°C)	ΔH_m (J/g)	χ (%)
PC08	*-48.0*	*22.3*	*173.7*	*58.4*	*102.2*	*75.1*
PC12	*-47.4*	*20.6*	*128.2*	*57.8*	*101.6*	*74.7*
PC17	*-47.2*	*18.8*	*98.7*	*57.1*	*100.1*	*73.6*
HPC08	*-47.5*	*30.8*	*81.7*	*59.8*	*76.4*	*56.2*
HPC12	*-48.3*	*27.7*	*67.7*	*60.9*	*75.8*	*55.7*
HPC17	*-48.4*	*27.5*	*53.2*	*62.0*	*68.6*	*50.4*

HAVE YOU TAKEN INTO ACCOUNT THE FACT THAT HPCs CONTAIN ONLY 7/10 OF PCL FOR THE SAME MASS ? THEREFORE TO HAVE A FAIR COMPARISON (BECAUSE ALL THE ΔH ARE NORMALISED PER MASS, BUT FOR HPCs THE MELTING PEAK IS RELATED TO 7/10 OF THIS MASS) I BELIEVE (BUT MAYBE YOU SHOULD CHECK AS I AM NOT A DSC EXPERT) THAT χ HAS TO BE DIVIDED BY 7/10 ; IF SO, THE χ REMAINS NEARLY UNCHANGED FOR PCLs AND HPCs

In terms of crystallinity differences, printing was also found to have a negligible effect, while a minor reduction was assessed after hybrid synthesis. The degree of crystallinity of as-purchased polymers was relatively high (~ 75 %). However, a reduction of circa 33 % was observed after the sol-gel process. Most likely, the interpenetrated silicate network causes a reduction in the possibility of polymer chains to successfully pack and, as a consequence, a decrease in crystallinity. Besides the analysis of PCL differences, the highlight of the DSC analysis was the detection of an intense new set of peaks centered around 150 °C following sol-gel synthesis. These peaks appear only on H1 and are absent in H2. In addition, the printing process seems to affect the peak temperature and intensity (**Figure 4**).

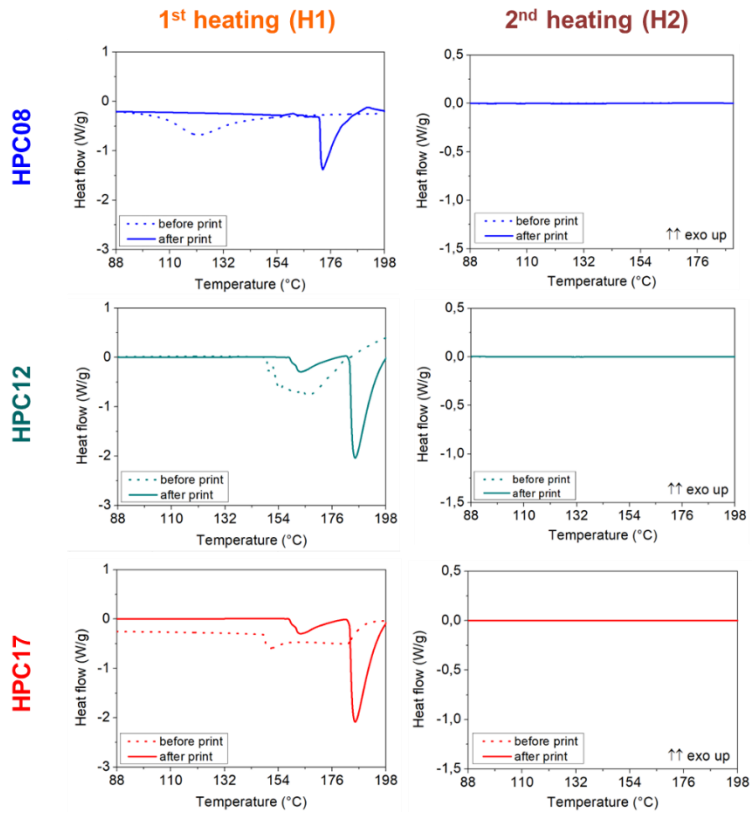

Figure 4: DSC results showing the silanols condensation peaks (~ 120-180 °C) during H1 and H2. Note how peaks completely disappear on H2. This peak is in fact highly susceptible to thermal treatments: H1 determines the condensation of all residual silanols. Significant variations also occur as a consequence of printing.

The overall shape of the band is also significantly variable. Taken collectively, these observations suggest that this peak group is due to temperature-catalyzed condensation of remaining silanols within the hybrid. This hypothesis is consistent with the result of rheology and TGA performed in parallel (see paragraphs 3.1.2 and 3.1.3). It is also backed up by other investigation suggesting the occurrence of such phenomenon in sol-gel based silica[43–45]. In particular, the effectiveness of thermal treatments (such as FDM) in reducing the peak area at 150 °C is well reported[43]. The reduction is proportional to the heating temperature. The silanol condensation peaks were observed in three different configurations: (i) H1, before printing: the peak is at relatively lower temperature, in particular in the case of HPC08, were it sets around 120 °C. Its different shape suggests that it might be also due to the evaporation of residual solvents; (ii) H1, post-printing: the peak sharpens and shifts to higher temperatures (~ 185 °C); (iii) H2: no peak detected. All the residual silanols reacted during H1. This result indicates that the transformation causing the peak is irreversible. The intensity of the silanol condensation peak can be reduced by increasing aging time. However, longer aging also results in high variations in rheological behavior, ultimately hampering printing. For this reason, longer aging time might not be a suitable strategy for the envisaged application. In practical terms, the results of the DSC analysis suggest optimizing the 3D printing of O/I hybrids at temperatures that sit below 100 °C. In this way, the desired printing properties can be maintained, avoiding, or at least delaying as long as possible, permanent temperature-dependent changes in the material.

3.2 Printability of PCL/BG hybrids

Thanks to a thorough investigation of the parameters affecting 3D printing, successful printing of O/I hybrids can be reported for the first time using a material based on PCL and binary BG. Figure 5 shows a typical array of printed scaffolds used to investigate the reproducibility of the printing process of the PCL/BG hybrids synthesized in this study.

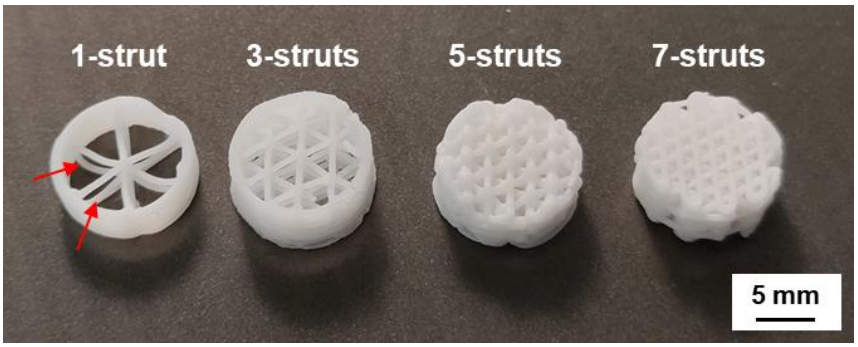

Figure 5: Investigation into the printability of HPC17. The effect of strut distance on the overall quality of printing is assessed. Red arrows highlight the collapse occurring on 1-strut structures.

Samples with decreasing strand distance were fabricated to assess material integrity and identify possible collapse of strands in the case of wide inter-strand distance. Remarkable printability with results comparable to pure PCL was observed for PCL/BG hybrids. Scaffolds with 3, 5 and 7 strands per layer did not show any sign of collapse. Only minor bending of the strands was observed in samples with one strand per layer (see Figure 5, red arrows). However, due to the improbability of such a printing scenario, the result can be considered non-critical. Careful tailoring of the printing parameters, in particular keeping cartridge and nozzle temperatures as low as possible, is of chief importance to grant reproducibility. Temperatures exceeding 100 °C result in printing inhomogeneity. Moreover, the choice of polymer was found to play an important role. Previous trials using wide-use PCLs from other suppliers gave poor results (data not shown). This is most probably due to higher MW and PD of those polymers compared to the ones used in this study.

The results of the morphological analysis showed regular, homogeneous woodpile structures for all three PCLs and their hybrids. Interestingly, while PCL struts show a completely smooth surface (Figure 6, top-middle panel), hybrid ones are characterized by a marked surface roughness (Figure 6, bottom-middle panel). Only few particle-like features are observed, confirming that hybrid synthesis was successful in producing a single-phase material, as already observed with rheology (see Section 3.1.3), and not a conventional composite with micro-sized silica particles dispersed within a polymeric matrix.

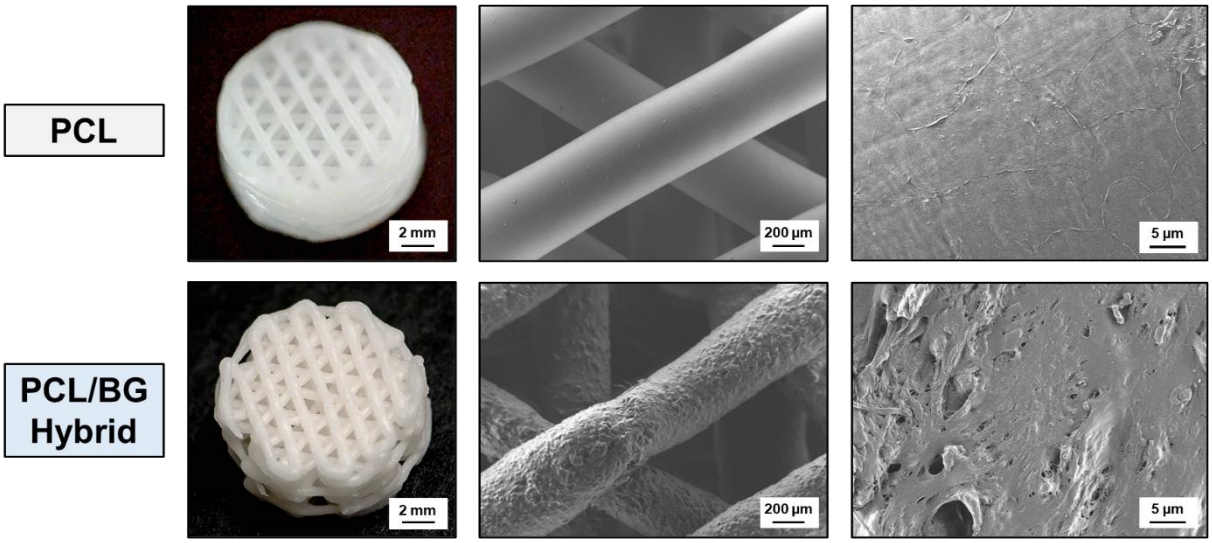

Figure 6: Typical morphologies of PCL and PCL/BG hybrid scaffolds captured with an optical microscope and an SEM (middle and right, at 100X and 2.000X, respectively). The specimens shown in the images are PC17 and HPC17, other samples showed comparable features.

All polymers chosen in this study offer a good range of thermal and rheological properties to produce printable hybrids, while being also printable as stand-alone materials, albeit with some necessary adjustments in the printing temperature (Table 1). Although an increase in temperature would be expected to decrease the viscosity of the molten material, the opposite phenomenon occurs. As demonstrated by rheology, increasing temperature above 100 °C significantly and negatively affects printability most presumably as a consequence of residual silanols condensation, or solvent evaporation: the inorganic network of the hybrid increases in connectivity, boosting viscosity. Printing attempts above 100 °C caused frequent nozzle clogging. Therefore, for successful FDM of PCL/BG hybrids it is of chief importance to print at the lowest possible temperature.

3.3 Scaffold stability in simulated body fluid

Adequate in vitro stability and apatite-forming ability of PCL/BG hybrid scaffolds are key elements toward the use of materials in orthopedics and other related biomedical applications. In particular, immersion tests in simulated body fluid (SBF) were performed aiming to verify that the processing technique (i.e., FDM) does not significantly alter the behavior of the hybrids in a physiological environment. PCL/BG hybrids are in fact characterized by an ideal degradation rate and the ability to rapidly enhance apatite deposition. Previously reported degradation assays confirmed that PCL/BG scaffolds prepared with solvent-based techniques are relatively stable in SBF, showing a weight variation below 5 % until 3 weeks of immersion, increasing to 10 % after one month[15]. More importantly, a significant layer of apatite was observed within days of contact with SBF[15,16]. To assess possible effects of the FDM process, pH and weight variation of all formulations were monitored during a period of 3 weeks. In parallel, samples of scaffolds were retrieved at selected time points (1, 3, 7, 14 and 21 days) and analyzed to identify clues of apatite formation.

Almost no variation in pH was observed compared to an SBF control (i.e., a minor increase from 7.4 to 7.7 over the tested period). The only notable difference between PCLs and hybrids is a minor buffer effect, probably due to ion release from the inorganic component of the hybrids (Figure 7).

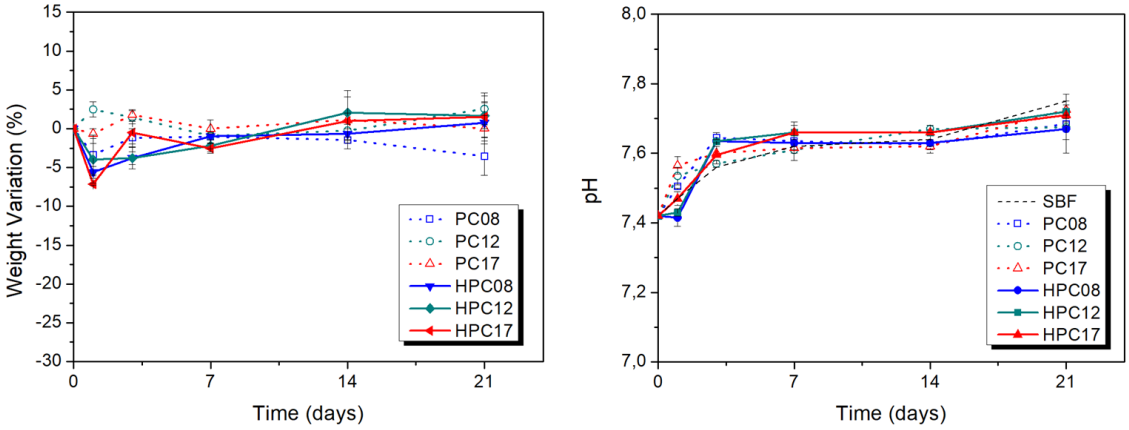

Figure 7: Weight (left) and pH (right) variations of 3D printed samples of the three PCLs and their hybrids immersed in SBF for up to 21 days.

The buffer effect occurs only after one day of immersion: hybrids seem to maintain the pH of SBF at 7.4 longer than PCL samples. From day 3, however, all samples follow the same trend. Weight variations over the same period were also negligible (Figure 7). These results are in contrast to previous studies on similar materials, where a decrease in weight was observed[15,46,47]. However, materials in these studies were processed using solvent-based techniques. It is reasonable to think that heating-based processing methods such as FDM would result in increased chain packing and could consequently reduce the swelling and degradation rate of the scaffold[48].

Hybrid 3D printed scaffolds are bioactive

After evaluating the stability in physiological fluids, it was essential to confirm that the previously reported fast and strong apatite forming ability of PCL/BG hybrids was preserved after printing. A multifaceted analysis was performed using ICP-OES, SEM, EDX and PIXE. The ion release from the samples and the associated deposition of calcium phosphates on their surface were investigated and characterized in SBF over various periods of time up to three weeks.

The evolution of Ca, P and Si concentrations in SBF as a function of interaction time is reported in Figure 8A-C for the three tested formulations. No significant difference was observed depending on the PCL used. This result could be expected considering that the monitored ions are delivered from the inorganic component of the hybrid. ICP-OES results show a trend that is known to be typical for the interaction between BGs and SBF[49]. At the first periods of measurement, Ca and Si are released from the hybrid matrix, resulting in an increase of their concentration in the medium. These two ions are known to have a substantial role in changing the local ion supersaturation of SBF, consequently triggering apatite precipitation. Particularly, Si was reported to act as nucleation agent, while Ca improves crystal growth[50]. In addition, Ca and Si are also known to elicit an osteostimulative effect on osteoblast, improving their proliferation and differentiation[51–53].

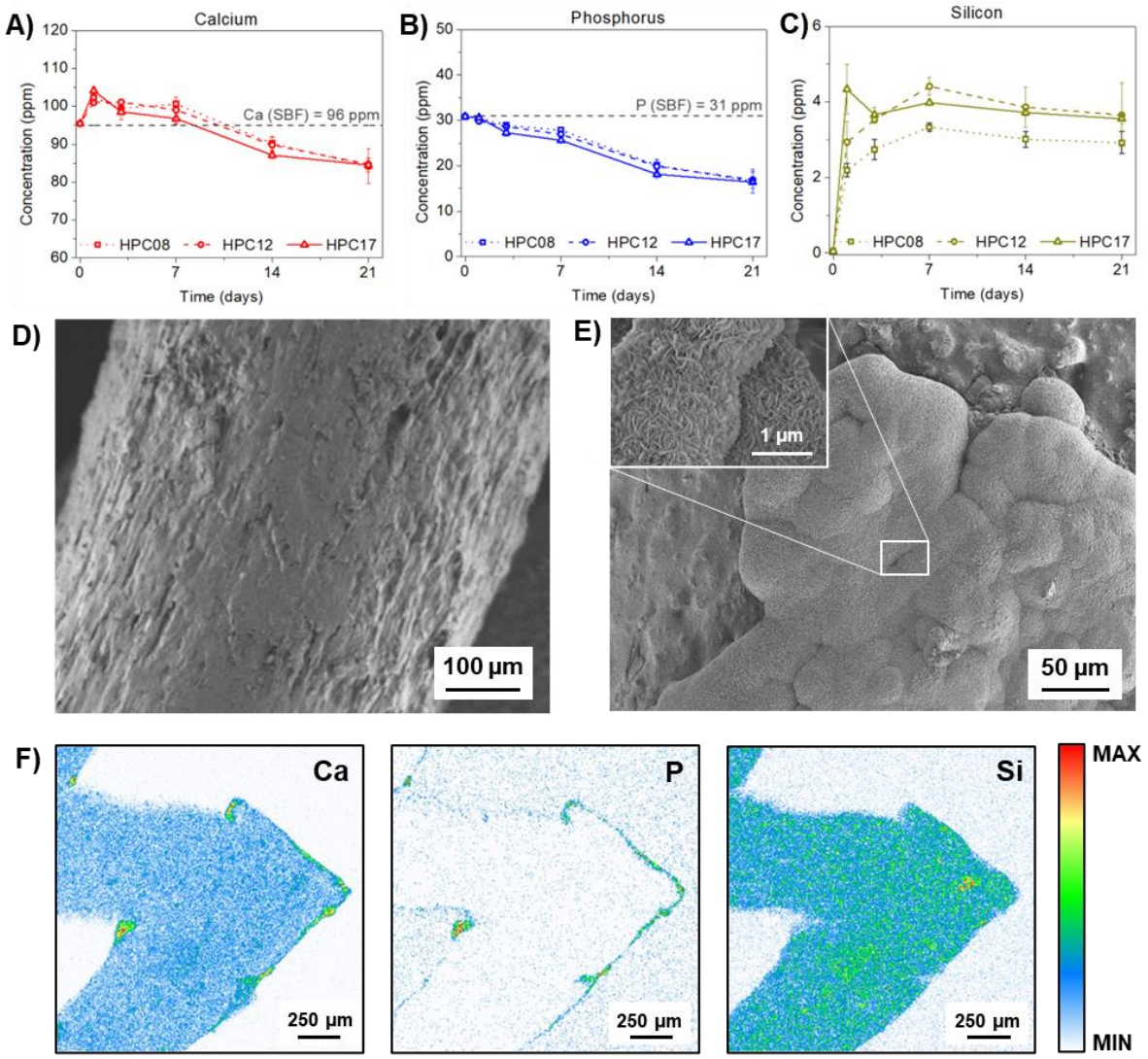

Figure 8: A-C) Ion release in SBF from the three formulations of PCL/BG 3D printed hybrid scaffolds tested in this study (initial concentration of Ca and P in SBF also shown). SEM images of a HPC17 sample show the typical morphology of the scaffolds D) before and (E) after 21 days in SBF (EDX spectrum also shown): note the apatite-like crystals forming on the surface of the material. F) PIXE chemical imaging of Ca, P and Si inside a HPC17 cross-section (21 days in SBF).

Since the samples contain no P, no initial burst peak is observed for this element. After the initial stages of ion release, Si concentration remains relatively uniform at about 3-4 ppm. The amount of Ca and P in SBF, on the other hand, decrease with incubation time from 95 to 80 ppm and from 31 to 16 ppm after 21 days, respectively. This can be ascribed to the onsetting of CaP precipitation on the material's surface. Compared to the results obtained with different techniques[15], the ion release of 3D printed scaffolds follows the same trend. However, in the case of Ca and P the release rate is highly reduced (i.e., a comparable reduction occurs over a period of a few days instead of a few weeks). The concentration of silicon on the other hand follows a similar trend, but with a significantly lowered plateau (few ppm instead of ~ 50 ppm for highly porous scaffolds). Both variations are most probably a consequence of the compacting of the material following the thermal processing of FDM: while solvent-processed PCL/BG hybrids are characterized by widespread microporosity[15,16] and overall higher total porosity (~80%), 3D printed ones are compact and contain less unreacted Si, as previously confirmed by DSC and rheology.

They nevertheless possess sufficient surface roughness (Figure 8D) and ion release to trigger the formation of apatite crystals arranged in a characteristic cauliflower-like structure on the scaffolds, as confirmed by SEM (Figure 8E). The presence of Ca and P in these structures was qualitative confirmed by EDX (bottom left inset of Figure 8E, for more information see supplementary data). These observations were also corroborated by quantitative chemical mapping. PIXE and the nuclear microprobe were used to identify regions of CaP deposition on scaffolds at 21 days in SBF and confirm that these areas were characterized by the correct Ca/P ratio to describe them as apatite. The average Ca/P atomic ratio of the deposits is 1.9 ± 0.2. The value is slightly higher than the theoretical Ca/P ratio of stoichiometric HA (1.67), but it is fully compatible with reported values measured for bones (1.7 - 2.1)[54] and "biological" HA, which both consist of nanocrystalline non-stoichiometric HA. The deposits are mainly found on the surface of the scaffolds, wedged in corners and cracks that are acting as nucleation sites. This result is in contrast with previously reported studies that showed how PCL/BG hybrids could enhance apatite deposition even inside the bulk of the material[15]. This property was previously associated with the characteristic homogeneous incorporation of Ca inside O/I hybrids compared to other bioactive materials[8]. However, these new results highlight that this property is not intrinsic of PCL/BG hybrids but also depend on the processing technique. Hence, the difference is most probably a consequence of the low porosity and high density of scaffolds as a result of the printing process, compared to previously explored solvent-based fabrication methods[8,15]. Nevertheless, 3D printed PCL/BG hybrids remain significantly bioactive, showing the typical apatite formation ability of benchmark materials used in orthopedic applications, such as HA and BG composites[5,55].

4. Concluding remarks

In this work, we reported the direct 3D printing of PCL/BG hybrids using a fused deposition modelling approach. To our knowledge, this is the first time an organic/inorganic hybrid material is successfully processed into 3D scaffolds from powder without additional fabrication steps and without the need for solvents. The parameters to optimize the printability of PCL/BG hybrids were successfully identified. In particular, valuable technical insights were drawn from the results of the thermophysical characterization. It was confirmed that the fabrication process (sol-gel synthesis and subsequent post-processing) induces relatively low degradative stress to the polymer. Increases in viable printing temperatures were generally associated with polymer with higher MW. In addition, evidence that a more interconnected silica network can highly damage the printability was also found. For these reasons, both (1) the aging of the gelled hybrid (max 1 h) and (2) the printing temperature (<100 °C) should be minimized. Controlling these two variables results in a more polymer-like rheological behavior and in longer viable printing times, respectively. After proving suitable printability and offering an in-depth investigation of its processing parameters, printed scaffolds were also analyzed in terms of bioactivity. In particular, the preservation of the native bioactivity of the hybrid after printing was assessed. Results confirmed that direct 3D printed PCL/BG hybrid scaffolds are stable in a physiological-like environment and are able to promote the deposition of formation of apatite on their surface, alas with slower kinetics compared to scaffolds of the same material fabricated using solvent-based techniques. Our findings provide valuable guidelines to help researchers towards the correct choice of polymer and printing parameters for successful hybrid FDM. By carefully controlling the printing variables as previously described, scaffolds can be prepared in a reproducible and high-throughput manner from a stable precursor (hybrid powder), offering significant advantages compared to direct printing from sol (e.g., more reproducible, more working time) or to convoluted indirect methods. Improved reproducibility is the first key step

towards the systematic application of 3D printed O/I hybrid scaffolds in bone repair and tissue engineering. Now that the printability and bioactivity of PCL/BG hybrids are confirmed, the next steps will also include the mechanical and biological characterization of these scaffolds in view of their application for bone repair and regeneration.

Acknowledgements

This project has received funding by the EU under the European Regional Development Fund (ERDF) program ("Fonds Européen de Développement Régional" FEDER) and Région Auvergne-Rhône-Alpes under the "pack Ambition Recherche" program (BIOSTEON project, grant agreement No. AV0016426), and the Agence Nationale de la Recherche of the French government through the program ''Investissements d'Avenir'' (16-IDEX-0001 CAP 20-25, Hub Innovergne project). The authors would like to thank…

Conflict of Interest

The authors declare no conflict of interest.

References

[1] S. Bose, D. Ke, H. Sahasrabudhe, A. Bandyopadhyay, *Prog. Mater. Sci.* **2018**, *93*, 45.

[2] D. Puppi, F. Chiellini, *Appl. Mater. Today* **2020**, *20*, 100700.

[3] K. Pielichowska, S. Blazewicz, in *Adv. Polym. Sci.*, **2010**, pp. 97–207.

[4] A. R. Boccaccini, M. Erol, W. J. Stark, D. Mohn, Z. Hong, J. F. Mano, *Compos. Sci. Technol.* **2010**, *70*, 1764.

[5] L. Gritsch, E. Perrin, J.-M. Chenal, Y. Fredholm, A. L. Maçon, J. Chevalier, A. R. Boccaccini, *Appl. Mater. Today* **2021**, *22*, 100923.

[6] J. Jones, *Acta Biomater.* **2013**, *9*, 4457.

[7] B. M. Novak, *Adv. Mater.* **1993**, *5*, 422.

[8] J. Lao, X. Dieudonné, F. Fayon, V. Montouillout, E. Jallot, *J. Mater. Chem. B* **2016**, *4*, 2486.

[9] R. D. Greenhalgh, W. S. Ambler, S. J. Quinn, E. S. Medeiros, M. Anderson, B. Gore, A. Menner, A. Bismarck, X. Li, N. Tirelli, et al., *J. Mater. Sci.* **2017**, *52*, 9066.

[10] X. Dieudonné, V. Montouillout, É. Jallot, F. Fayon, J. Lao, *Chem. Commun.* **2014**, *50*, 8701.

[11] L. S. Connell, F. Romer, M. Suárez, E. M. Valliant, Z. Zhang, P. D. Lee, M. E. Smith, J. V. Hanna, J. R. Jones, *J. Mater. Chem. B* **2014**, *2*, 668.

[12] Y. Shirosaki, T. Okayama, K. Tsuru, S. Hayakawa, A. Osaka, *Chem. Eng. J.* **2008**, *137*, 122.

[13] Y. Vueva, L. S. Connell, S. Chayanun, D. Wang, D. S. McPhail, F. Romer, J. V. Hanna, J. R. Jones, *Appl. Mater. Today* **2018**, *11*, 1.

[14] M.-Y. Koh, C. Ohtsuki, T. Miyazaki, *J. Biomater. Appl.* **2011**, *25*, 581.

[15] C. Bossard, H. Granel, Y. Wittrant, É. Jallot, J. Lao, C. Vial, H. Tiainen, *Biomed. Glas.* **2018**, *4*, 108.

[16] H. Granel, C. Bossard, A.-M. Collignon, F. Wauquier, J. Lesieur, G. Y. Rochefort, E. Jallot, J. Lao, Y. Wittrant, *ACS Appl. Bio Mater.* **2019**, *2*, acsabm.9b00407.

[17] Y. Ding, W. Li, D. W. Schubert, A. R. Boccaccini, J. A. Roether, H. A. Santos, *Mater. Sci. Eng. C* **2021**, *124*, 112079.

[18] L. Liu, C. Li, Y. Jiao, G. Jiang, J. Mao, F. Wang, L. Wang, *Polym. Test.* **2020**, *91*, 106798.

[19] F. Tallia, L. Russo, S. Li, A. L. H. Orrin, X. Shi, S. Chen, J. A. M. Steele, S. Meille, J. Chevalier, P. D. Lee, et al., *Mater. Horizons* **2018**, *5*, 849.

[20] E. Shukrun, I. Cooperstein, S. Magdassi, *Adv. Sci.* **2018**, *5*, 1800061.

[21] S. Hendrikx, C. Kascholke, T. Flath, D. Schumann, M. Gressenbuch, F. P. Schulze, M. C. Hacker, M. Schulz-Siegmund, *Acta Biomater.* **2016**, *35*, 318.

[22] D. W. Chae, Y. Nam, S. G. An, C. G. Cho, E. J. Lee, B. C. Kim, *Korea-Australia Rheol. J.* **2017**, *29*, 129.

[23] J. Isaac, J. Nohra, J. Lao, E. Jallot, J.-M. Nedelec, A. Berdal, J.-M. Sautier, *Eur. Cells Mater.* **2011**, *21*, 130.

[24] P. S. Kandelousi, S. M. Rabiee, M. Jahanshahi, F. Nasiri, *J. Bioact. Compat. Polym.* **2019**, *34*, 97.

[25] K. T. Shalumon, K. H. Anulekha, C. M. Girish, R. Prasanth, S. V. Nair, R. Jayakumar, *Carbohydr. Polym.* **2010**, *80*, 413.

[26] M. Bohner, J. Lemaitre, *Biomaterials* **2009**, *30*, 2175.
[27] A. L. B. Maçon, T. B. Kim, E. M. Valliant, K. Goetschius, R. K. Brow, D. E. Day, A. Hoppe, A. R. Boccaccini, I. Y. Kim, C. Ohtsuki, et al., *J. Mater. Sci. Mater. Med.* **2015**, *26*, 1.
[28] F. Mirani, A. Maffini, F. Casamichiela, A. Pazzaglia, A. Formenti, D. Dellasega, V. Russo, D. Vavassori, D. Bortot, M. Huault, et al., *Sci. Adv.* **2021**, *7*, DOI 10.1126/sciadv.abc8660.
[29] O. Persenaire, M. Alexandre, P. Degée, P. Dubois, *Biomacromolecules* **2001**, *2*, 288.
[30] Y. Ding, J. A. Roether, A. R. Boccaccini, D. W. Schubert, *Eur. Polym. J.* **2014**, *55*, 222.
[31] Y. Ding, W. Li, T. Müller, D. W. Schubert, A. R. Boccaccini, Q. Yao, J. A. Roether, *ACS Appl. Mater. Interfaces* **2016**, *8*, 17098.
[32] W.-J. Jeong, H. Nishikawa, H. Gotoh, T. Takemoto, *Mater. Trans.* **2005**, *46*, 704.
[33] R. U. Rao, K. N. S. Suman, V. V. S. K. Rao, K. Bhanukiran, *Int. J. Engin. Sci. Techn.* **2011**, *3*, 6259.
[34] C. A. Kelly, S. H. Murphy, G. A. Leeke, S. M. Howdle, K. M. Shakesheff, M. J. Jenkins, *Eur. Polym. J.* **2013**, *49*, 464.
[35] A. L. Arraiza, J. R. Sarasua, J. Verdu, X. Colin, *Int. Polym. Process.* **2007**, *22*, 389.
[36] D. W. Chae, Y. Nam, S. G. An, C. G. Cho, E. J. Lee, B. C. Kim, *Korea-Australia Rheol. J.* **2017**, *29*, 129.
[37] N. C. Paxton, J. Ren, M. J. Ainsworth, A. K. Solanki, J. R. Jones, M. C. Allenby, M. M. Stevens, M. A. Woodruff, *Macromol. Rapid Commun.* **2019**, *40*, 1900019.
[38] A. Mohamed, V. L. Finkenstadt, S. H. Gordon, G. Biresaw, D. E. Palmquist, P. Rayas-Duarte, *J. Appl. Polym. Sci.* **2008**, *110*, 3256.
[39] V. Speranza, A. Sorrentino, F. De Santis, R. Pantani, *Sci. World J.* **2014**, *2014*, 1.
[40] P. J. Sánchez-Soto, J. M. Ginés, M. J. Arias, C. Novák, A. Ruiz-Conde, *J. Therm. Anal. Calorim.* **2002**, *67*, 189.
[41] S. H. Murphy, G. A. Leeke, M. J. Jenkins, *J. Therm. Anal. Calorim.* **2012**, *107*, 669.
[42] K. Phillipson, Ageing and Crystallisation of Polycaprolactone Doctor of Philosophy, **2014**.
[43] F. Rubio, J. Rubio, J. L. Oteo, *Thermochim. Acta* **1998**, *320*, 231.
[44] W. Chen, H. Feng, D. He, C. Ye, *J. Appl. Polym. Sci.* **1998**, *67*, 139.
[45] F. Rubio, J. Rubio, J. L. Oteo, *Thermochim. Acta* **1997**, *307*, 51.
[46] D. Mondal, S. J. Dixon, K. Mequanint, A. S. Rizkalla, *J. Mech. Behav. Biomed. Mater.* **2017**, *75*, 180.
[47] B. A. Allo, A. S. Rizkalla, K. Mequanint, *Langmuir* **2010**, *26*, 18340.
[48] A. Haider, S. Haider, M. Rao Kummara, T. Kamal, A.-A. A. Alghyamah, F. Jan Iftikhar, B. Bano, N. Khan, M. Amjid Afridi, S. Soo Han, et al., *J. Saudi Chem. Soc.* **2020**, *24*, 186.
[49] C. Ohtsuki, T. Kokubo, T. Yamamuro, *J. Non. Cryst. Solids* **1992**, *143*, 84.
[50] M. Mozafari, A. Ramedani, Y. N. Zhang, D. K. Mills, in *Thin Film Coatings Biomater. Biomed. Appl.*, Elsevier, **2016**, pp. 167–195.
[51] S. Maeno, Y. Niki, H. Matsumoto, H. Morioka, T. Yatabe, A. Funayama, Y. Toyama, T. Taguchi, J. Tanaka, *Biomaterials* **2005**, *26*, 4847.
[52] E. J. Kim, S. Y. Bu, M. K. Sung, M. K. Choi, *Biol. Trace Elem. Res.* **2013**, *152*, 105.
[53] S. Zou, D. Ireland, R. A. Brooks, N. Rushton, S. Best, *J. Biomed. Mater. Res. Part B Appl. Biomater.* **2008**, *90B*, 123.
[54] M. Tzaphlidou, R. Speller, G. Royle, J. Griffiths, *Phys. Med. Biol.* **2006**, *51*, 1849.
[55] F. Baino, G. Novajra, C. Vitale-Brovarone, *Front. Bioeng. Biotechnol.* **2015**, *3*, 202.